55th CIRP Conference on Manufacturing Systems

Multi-physics based methodology for evaluating powder feeding quality for Laser Metal Deposition

Stefano Baraldo[a]*, Alessandro Roncoroni[a], Filippo Palo[b], Anna Valente[a]

aSUPSI, Institute of Systems and Technologies for Sustainable Production, via La Santa 1, Lugano-Viganello 6962, Switzerland
bXC Engineering srl, via Matteotti 7, Cantù 22063, Italy

* Corresponding author. Tel.: +41 (0)58 666 6698. *E-mail address:* stefano.baraldo@supsi.ch

Abstract

Powder based Laser Metal Deposition (LMD) is an additive manufacturing technology that offers great advantages to the production of high added value products, like the possibility to manufacture in one whole piece parts with very complex geometries, or to repair existing ones. One of the critical elements of this technology is the powder feeding system, which, depending on its specific design, can provide powder flows that are more or less stable, thus heavily affecting the homogeneity of deposited tracks and, ultimately, of final part quality.

In this work, we propose a methodology for assessing the fitness of a powder feeder for a LMD system. The assessment is based on *deposition quality maps*, which provide a reference for predicting the waviness of a deposited track in function of powder flow oscillation frequency and amplitude. Such maps are generated by performing multi-physics simulations of straight deposition tracks and evaluating their level of regularity. The simulation model is calibrated by a preliminary experimental campaign and can be used further on to assess the effects that any flow frequency-amplitude couple has on deposition quality, without the need to perform new deposition experiments for assessing a new powder feeder. The methodology is demonstrated by calibrating the simulation model for a commercial LMD machine loaded with Inconel 718 powders.

1. Introduction

Laser Metal Deposition (LMD) is an additive manufacturing technology that exploits a laser beam to melt powders, which are carried on a target substrate by a gas stream. The fused powder generates a *melt pool*, i.e. a drop of molten metal that evolves into a solid track when the deposition head is moved forward and the metal cools down [1]. This process is an enabler for producing many complex geometries and for repairing metal parts, while maintaining high mechanical performances [2].

One of the key elements of such a complex technology is the powder feeding system. Depending on the specific type of feeding mechanism (e.g. rotating disk, drum, cochlea, vibration-based, Venturi-based [3]) and on its performance, the powder flow emitted by the deposition head can be more or less stationary, heavily affecting the final part quality. Evaluating the characteristic behavior of a powder feeder in relation to a specific LMD machine is therefore of paramount importance for guaranteeing high quality parts.

In this work, we propose a methodology for assessing the fitness of a powder feeder to a LMD system. The assessment is performed by introducing the *Deposition Quality Map* (DQM), a new type of diagnostic tool that provides the values of track waviness indices, depending on the powder flow oscillation frequency and amplitude. The DQMs are generated thanks to a numerical model of the LMD process, which allows to simulate the deposition of tracks and to evaluate their level of regularity.

The model is calibrated for the target LMD machine by a preliminary experimental campaign, which can be performed with any available powder feeder, and it can be used further on to assess the effects that any flow frequency-amplitude couple has on deposition quality, without the need to perform deposition experiments for assessing a new powder feeder. The whole pipeline is illustrated in Fig. 1.

The article is structured as follows. Sec. 2 describes the LMD multi-physics modelling and computational approach adopted in this work. Sec. 3 introduces the track quality metrics used to create DQMs. Sec. 4 presents the results obtained by calibrating the model on a real LMD machine. Finally, Sec. 5 presents conclusions and comments on future works.

2. Multi-physics simulation of LMD

The implementation of accurate but efficient numerical models of LMD is still a major research topic, as the process is very complex and involves multiple phenomena (heat and mass transfer, fluid dynamics, thermo-mechanics, laser-matter interaction [4,5]) at multiple scales. Since our objective is the simulation of track geometries induced by powder flow fluctuations, we have chosen to accurately simulate only the phenomena that are considered critical to this aim. In particular, the full fluid dynamics of molten metal has been taken into account to properly predict deposition shape, and a particle model of incoming powder has been introduced. On the other side, the fluid dynamics of the carrier gas, the formation of internal stresses and the generation of different metallic microstructures have been neglected.

The simulation of the LMD process has been set up by relying on **FLOW-3D** [6], a multi-physics simulation software that implements finite volume methods and the Volume Of Fluid (VOF) [7] approach for treating free-surface CFD problems. The models solved in the proposed simulation set up are described in the following.
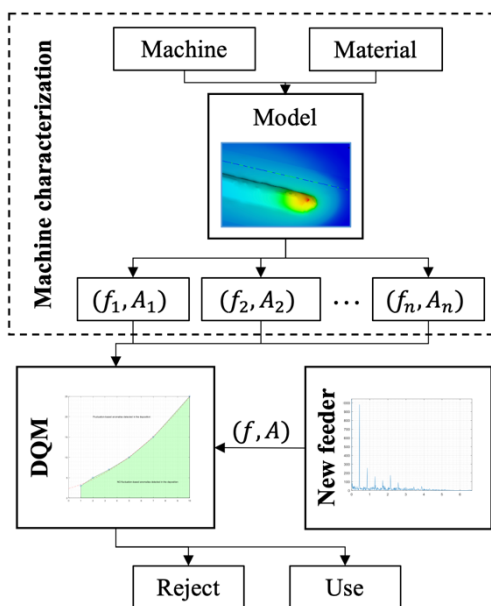

Fig. 1. Example of feeder assessment workflow. (f,A) indicates frequency-amplitude couples.

2.1. Continuity equations

Mass continuity for an incompressible flow is expressed by equation

$$\frac{\partial \rho}{\partial t} + \nabla \cdot (\rho \boldsymbol{v}) = 0,$$

where ρ is the fluid density and $\boldsymbol{v}$ is the fluid velocity vector.

Momentum continuity (Navier-Stokes equations) is expressed by

$$\frac{\partial \boldsymbol{v}}{\partial t} + (\boldsymbol{v} \cdot \nabla)\boldsymbol{v} = -\frac{1}{\rho}\nabla p + \frac{1}{\rho}\Delta(\mu\boldsymbol{v}) + \boldsymbol{g},$$

where p is pressure, μ is dynamic viscosity and $\boldsymbol{g}$ is the gravity acceleration vector. Both density ρ and dynamic viscosity μ are temperature-dependent, and in this work they are evaluated by a material-dependent look-up table.

The continuity equation of internal energy is

$$\frac{\partial}{\partial t}(\rho I) + \nabla \cdot (\rho \boldsymbol{v}I) = -p\nabla \cdot \boldsymbol{v} + \nabla \cdot (k\nabla T) + I_{SRC},$$

where I is internal energy, k is thermal conductivity and I_{SRC} is the energy source term (including viscous heating). Thermal conductivity is expressed as $k = \mu C_v / Pr$, where C_v is the specific heat at constant volume and Pr is the Prandtl number.

The internal energy I is expressed as

$$I = C_v \cdot T + (1 - f_s) \cdot \Delta H,$$

where f_s is the solid fraction and ΔH is the latent heat of fusion.

Finally, since the computational approach used in this work exploits the VOF method, also volume fraction continuity must be satisfied, by equation

$$\frac{\partial F}{\partial t} + \nabla \cdot (F\boldsymbol{v}) = F_{SOR},$$

where F represent the cell volume fraction occupied by the material (either solid or liquid). $F = 1$ means that the whole cell is filled by the material, $F = 0$ means that the cell is part of the *void* region, while all the values in-between identify free surface cells. The void region is the domain portion above the free surface, where the target material is absent, and it is modelled with simplified physics. In particular, carrier gas speed, temperature, pressure and density are specified as uniform, to determine the boundary conditions at the free surface and the forces acting on powder particles. The source term F_{SOR} is used to convert discrete particles to fluid material (see Sec. 2.4).

2.2. Boundary conditions

Heat transfer across wall-type boundaries is modelled by convection

$$q_w = hW_a(T_w - T_\infty),$$

where q_w is the heat flow through the wall, h is the convective coefficient, W_a is the wall surface area, T_w is wall temperature and T_∞ is the temperature of the external environment. The fluid-void heat transfer is governed by convection as well.

The radiative heat exchange with the void is computed as

$$q_{v,rad} = \varepsilon_v \sigma W_v \left(T_v{}^4 - T_\infty{}^4 \right),$$

where ε_v is surface emissivity, σ is the Stefan-Boltzmann constant, W_v is the surface area in contact with the void and T_v is the temperature of the fluid at the interface with the void.

Surface tension is applied at the free surface boundary, using a temperature-dependent surface tension coefficient.

2.3. Liquid-gas phase change

The mass transfer from free surface to void due to vaporization is expressed as a function of the surface temperature and of the pressures of liquid and vapor across it, following the model proposed in [8]:

$$m_{\text{trans}} = c \cdot \sqrt{\frac{M}{2\pi R T_{\text{surf}}}} \cdot (P_l^{\text{sat}} - P_v),$$

where M is the molecular weight of the vapor, c is an accommodation coefficient, R is the vapor gas constant, T_{body} is the average liquid temperature on the bubble surface, P_l^{sat} is the pressure of the liquid state (corresponding to the saturation pressure) and P_v is the pressure of the vapor state.

2.4. Discrete particles model

A Lagrangian model is adopted to describe the inlet of discrete powder particles into the computational domain. The particles can carry and transfer heat and momentum to the fluid, melt, solidify and evaporate, but they cannot interact with each other, as simplifying assumption.

The motion of particles is modelled with Newton's second law. Considering each particle as a sphere, its acceleration is computed as

$$\frac{d\boldsymbol{v}_p}{dt} = -\frac{1}{\rho_p}\nabla p + \boldsymbol{g} + \beta(\boldsymbol{v} - \boldsymbol{v}_p)|\boldsymbol{v} - \boldsymbol{v}_p|\frac{\rho}{\rho_p}$$
$$+ \frac{m_{add}}{m_p}\left(\frac{d\boldsymbol{v}}{dt} - \frac{d\boldsymbol{v}_p}{dt}\right),$$

where $\boldsymbol{v}_p$ is the particle velocity, $\boldsymbol{v}$ is the velocity of the carrier gas, ρ_p is the particle density, β is a drag force coefficient, m_p is the particle mass and m_{add} is the gas mass in a particle volume (according to Archimedes' law to compute the buoyancy force). β is calculated by empirical formulas based on the particle diameter and the Reynolds number.

The particles are introduced into the computational domain at the nozzles outlets, reproducing the average velocity of particles in the target application (see sec. 4.1). As mentioned in sec. 2.1, when a fused particle reaches the substrate, its volume is aggregated to the continuous fluid region, along with its other physical properties, thus forming the deposited track.

2.5. Laser beam and laser-material interaction

The laser beam is introduced as a heat flux at the free boundary. The power distribution is based on the considered laser source and optical path.

The value of absorptivity is considered as potentially different between particles and substrate, even in case they are made of the same material, to account for the spherical shape of particles and other phenomena that are not modelled explicitly. Both absorptivities have been set by starting from literature values and by tuning them basing on experimental results.

3. Deposition Quality Maps

In order to detect consistent fluctuations in the deposited tracks, the Fast Fourier Transform (FFT) in the space domain of the longitudinal height profile is computed. The FFT allows to obtain the profile spectrum, highlighting the *spatial frequencies* (thus expressed in mm^{-1}) where the most prominent peaks are present. The amplitude of such peaks is compared to the overall noise level in the transformed signal, to assess its significance.

Various frequency-amplitude combinations (f, A) of powder oscillations are simulated, representing different behaviors of powder flows. The spectrum of each track is then computed, and the significance of the highest peak is used to label the corresponding point in the (f, A) plane. The results of the FFT analysis in the spatial domain of the track section are collected in a frequency-amplitude map, the Deposition Quality Map (DQM), which shows the boundary between the zone of significant track height oscillations and the "safe zone", in which the powder flow oscillations do not affect the deposition.

3.1. Quality metrics

The approach described above is validated by computing the waviness along the centerline of simulated tracks, since we are interested in mm-scale defects, and by computing multiple roughness KPIs based on it, to assess if the FFT analysis reveals real geometric defects.

The used KPIs are based on roughness measures defined in ISO 4287 [9], while the parameters required to compute the roughness measures (cutoff wavelength, sampling length, total traverse length and evaluation length) have been set according with ISO 4288 [10]. In particular, the following KPIs have been considered, for the waviness profile (i.e. the low-pass filtered track height at its centerline):
- Ra, the mean absolute deviation $Z(x)$ from the mean of the roughness profile.
- Rz, the local maximum height of the profile over five sampling lengths.
- Rt, the distance between the highest peak and the deepest valley of the profile along the evaluation length.

A comparison between the curves generated under different process parameters allows to characterize the peak/valleys morphology in function of the powder flow fluctuation amplitude.
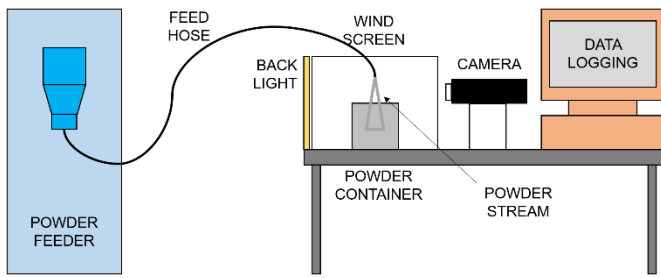
Fig. 2. Testing configuration for AM powder feeders.

4. Application

4.1. Experimental setup

The proposed methodology has been validated by assessing the influence of powder flow fluctuations on the deposition process, using typical fluctuation ranges measured on two different powder feeders, based respectively on rotating disk and vertical cochlea.

A test bench (Fig. 2) has been prepared to analyze the powder flow by artificial vision. The feeder in use releases powder inside a container where a strong backlight allows to clearly distinguish the flow by an industrial camera. Information about flow fluctuation amplitude and frequency are retrieved by visual processing of the powder flow video.

The feeder has been set with the following process parameters:

- Material: In718 spherical powder (mean grain diameter 77.5 μm);
- Carrier gas flow rate: 6 nlpm of argon 4.6;
- Powder feeding rate: variable from 40 g/min to 195 g/min.

It must be observed that the used range of powder feeding rates is higher than the typical operative conditions for LMD (about 6 g/min), in order to be detectable by the camera. Anyhow, recurrent pulsation frequencies and amplitudes (in % of nominal value) can be detected in the powder flow, independently of the discharge rate set. For this reason, we assume that the detected fluctuation is intrinsic to the feeding device and that it would appear also at lower discharge rates.

In order to extract frequency and amplitude information from the powders flow video, in each frame the average grey level over a ROI has been computed, as an indicator of the powder density (darker image = more powder). The obtained signal has been scaled to have mean equal to the nominal powder flow (measured with a scale basing on a 10-minutes emission). A sample result of this process is shown in Fig. 3.
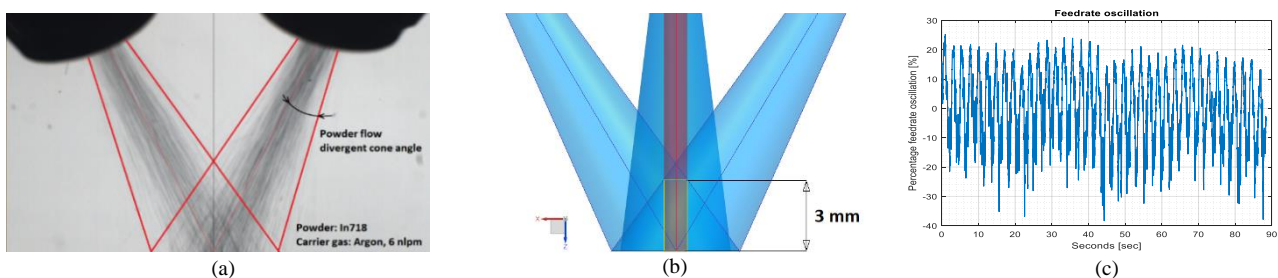
The aim of this experimental test is to identify a characteristic range of fluctuation frequencies and amplitudes of the powder flow. Observing the signal spectrums from the FFT of the powder flow signal computed from different samplings with both feeding devices, several frequency peaks from 0.4 Hz to about 10 Hz have been found.

The detected frequencies are used in the simulation, with the exception of frequencies below 1 Hz, since the time required to simulate a deposition long enough to appreciate such low frequencies would be too high to be used for practical purposes. However, since frequencies below 1 Hz provide a strong contribution to the fluctuation in terms of amplitude, a prediction will be proposed also at these low frequencies, extrapolating from available data.

The amplitude of oscillations, in accordance with the experimental results, range from ±2% to ±30%, therefore the same range has been used in simulation tests. As a result, the performed simulation campaign involved a factorial design of experiment on the following parameter values:

- Frequency: 1 Hz, 3 Hz, 5 Hz, 7 Hz, 10 Hz.
- Amplitude: ± 2%, 3%, 4%, 5%, 6%, 7%, 8%, 9%, 10%, 15%, 20%, 25%, 30%.

Such ranges, according to the experimental tests, allow obtaining a data grid sufficiently dense to cover the fluctuation range of the tested feeding devices (in amplitude and frequency).

4.2. Computational model setup

The reference experiments used in the proposed approach depositions of 20 mm straight single tracks of Inconel 718. In order to simulate this experiment, a box-shaped Cartesian domain of *45.32 mm x 27.32 mm x 8 mm* has been set.

Two meshes with different sizes have been defined: a larger one with coarse elements (0.75 mm edge size), for describing efficiently low gradients in the peripheral area, and a finer one (0.15 mm), nested in the middle of the computational domain (size 28 x 4 x 8 mm), where the deposition process is executed. The inner block has and "interblock" boundary condition at the interface with the outer block, i.e. values are interpolated and transferred to and from the coarser grid, while the external block has wall-type conditions on all the faces, except for the upper one, where atmospheric pressure has been set (Fig. 4).

The used machine is a Laserdyne 430, equipped with a 1080 nm Convergent CF1000 Nd:YAG laser source, of 1050 W max power. The beam has a Gaussian TEM00 distribution, which has a D86 diameter of 1 mm at the focal spot.
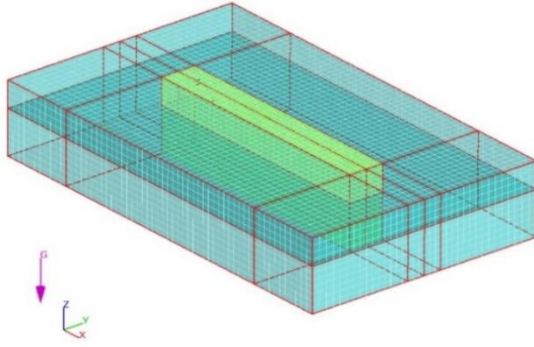

(a)	(b)	(c)

Fig. 3. (a) Powder flow video frame. (b) Laser-powder interaction distance. (c) Percentage powder flow oscillation (0% implies nominal powder flow).

Fig. 4. Computational domain.

Fig. 5. Simulated and real mean track profile for experiment P300F900.

The material properties used in the simulations are set for Inconel 718, which is the material used in the presented experiments, but the same information is required for any type of powder-substrate combination that must be tested.

For what concerns absorptivity, according to literature this complex interaction can be simplified for metals by tuning it within the range 0.15 - 0.5 [4], depending on the specific material and on surface quality. Since absorptivity has a large impact on deposition efficiency, it has been calibrated from from experiments, estimating different values for powders and substrate. A starting value of 0.35 has been used from literature, while final values have been reached after model tuning by comparison with real deposition experiments; the obtained, lower values reflect the need to account for unmodelled efficiency losses.

The test machine is equipped with a 4-nozzle deposition head, pointing towards a common spot. To reproduce it in the simulation, four discrete particle sources that move jointly with the laser beam have been set. The statistical distribution of particle diameters within the nominal range has been studied by optical microscopy, and implemented in the simulation. The output flow has been designed basing on the powder flow geometry (Fig. 3b); in particular, a particle-beam interaction length of 3 mm was determined, leading to the definition of a computational domain augmented with 3 mm of void region above the substrate.

The aforementioned simulation parameters are resumed in Table 1.

Table 1. Simulation parameters

Convection coefficient: h	20	$[W/(m^2 K)]$
Substrate absorptivity: α_{sub}	0.2	[-]
Particle absorptivity: α_{p}	0.18	[-]
Void temperature: T_{amb}	293	[K]
Void density	0.00166	$[g/cm^3]$
Powder diameter range	15-140	[μm]
Particle speed	4	m/s

4.3. Model calibration

The comparison between real and simulated single track geometries allows to assess the effectiveness of the proposed simulation approach and to tune the free model parameters, i.e. powder and substrate absorptivities.
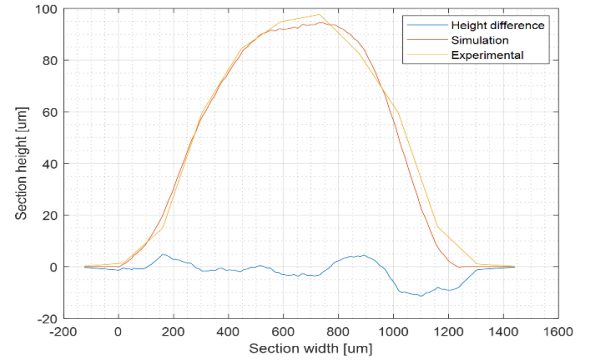
The experimental track profiles have been acquired with a Keyence VK-X-1000 confocal microscope, which can perform 3D scans up to 1 nm resolution. For each track, 10 equally-spaced transversal cutting planes have been defined; for each one of these cutting planes, a 2D track section profile has been generated. Finally, the mean of track height has been computed at each point of the transversal axis, averaging across the 10 available profiles. The same curves have been computed on the corresponding simulated track geometries, by using the volume fraction to delimit the free surface.

The metrics used for comparing the two cases are:
- $e_A = (A_{\text{sim}} - A_{\text{real}})/A_{\text{real}}$ relative error between mean section area of simulated and real track.
- $e_h = (h_{\text{sim}} - h_{\text{real}})/h_{\text{real}}$ relative error of peak height.
- $e_w = (w_{\text{sim}} - w_{\text{real}})/w_{\text{real}}$ relative error of peak width.
- $R = A_{\text{diff}}/A_{\text{real}}$, where A_{diff} is the area of the height difference between simulated and real profile.

The results obtained for three different velocity values with fixed power are reported in Table 2, while an exemplary comparison between simulated and measured track section is displayed in Fig. 5.

Table 2. KPIs of simulation-experiment geometry matching. P300F900 indicates a laser power of 300 W and a scanning velocity (machine feed rate) of 900 mm/min, etc.

	e_A	e_h	e_w	R
P300F900	3.93%	3.47%	0.55%	6.72%
P300F600	-11.92%	-12.42%	9.45%	13.21%
P300F350	16.93%	5.61%	2.16%	17.25%

Overall, the simulated profiles are very similar to the real ones, achieving a maximum error of 16.93% for what concerns the relative error of area on track P300F900. This is an indication that the implemented model has a good degree of generalizability to a wide range of velocities.

4.4. Deposition quality maps

The waviness maps for the three examined parameter settings visually validate the frequency-amplitude approach (Fig. 6): the shape and extension of the unsafe zones (top left corners) is coupled with a similar modification of the safe zone boundary. High frequency-high amplitude combinations yield wavier tracks at high velocities: in this case, the oscillation period translates into a longer spatial fluctuation, while lower velocities allow the heat affected zone to smooth out the height profile, thus resulting in a uniform geometry. An extreme case of this phenomenon is represented by 1 Hz oscillations, which
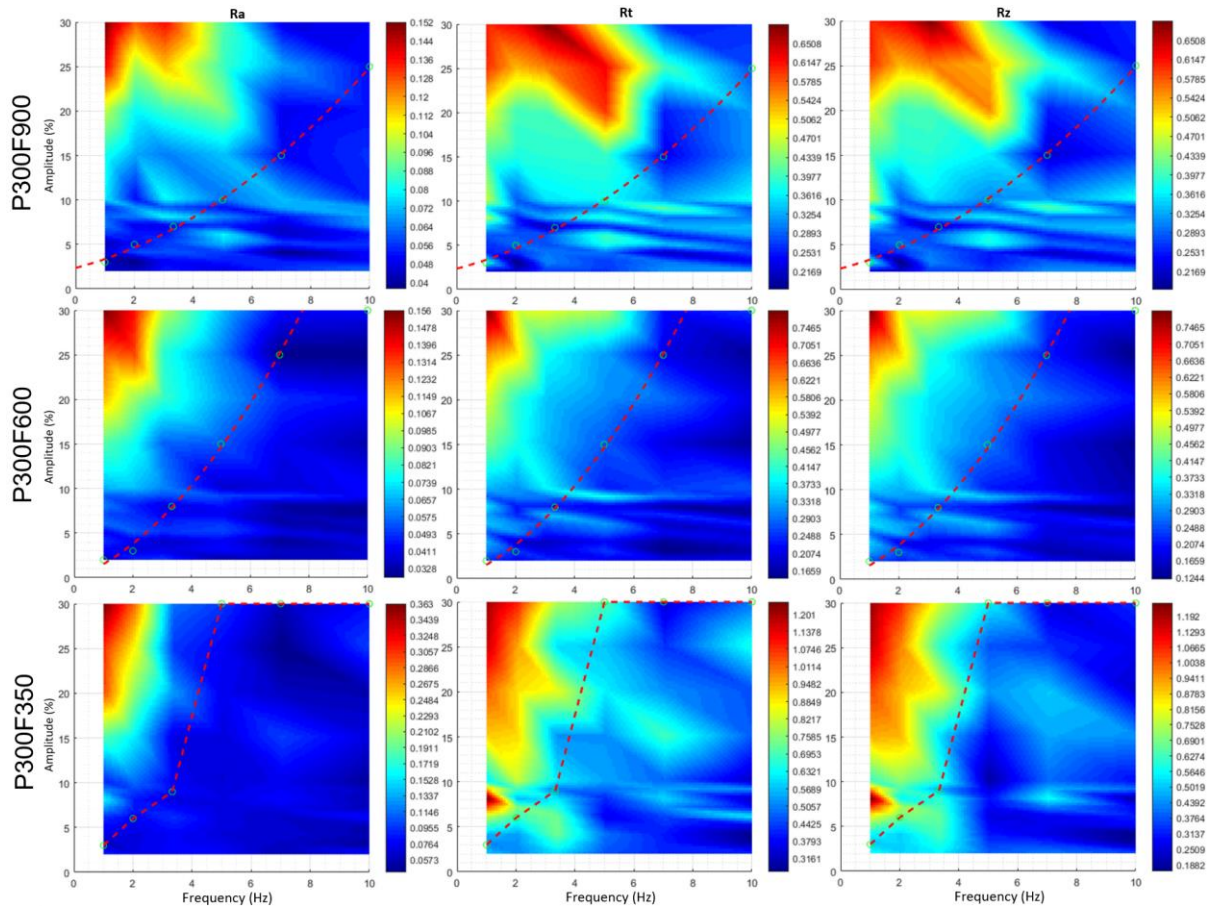
Fig. 6. Maps of Ra, Rt and Rz for the waviness profile of track P300F600. Dashed curves divide acceptability and non-acceptability regions.

generate significant waviness at any amplitude greater than 3%. The effect of amplitude is more difficult to predict, but the simulations allow to assess it and to avoid excluding devices with negligible oscillations for practical purposes.

5. Conclusions

This work proposes a methodology for assessing the maximum allowable powder feeding fluctuations, in terms of frequency and amplitude, obtain good quality tracks on a target LMD machine. Quality can be predicted for any frequency-amplitude couple, thanks to a comprehensive and accurate multi-physics simulation approach. The approach can be used as an effective decision tool to select powder feeding devices, without the need of actually testing it on the target machine.

Future works will include the refinement of model tuning, basing on a broader experimental campaign, and the generation of DQM for more process recipes and materials.

Acknowledgements

References

[1] Schmidt M, Merklein M, Bourell D, Dimitrov D, Hausotte T, Wegener K, Overmeye, L, Vollertsen F, Levy GN. Laser based additive manufacturing in industry and academia. CIRP Annals 2017; 66(2):561–583.

[2] Mazzucato F, Avram O, Valente A, Carpanzano E. Recent Advances Toward the Industrialization of metal Additive Manufacturing. In: Kenett RS, Swarz RS, Zonnenshain A, editors. Systems Engineering in the Fourth Industrial Revolution: Big Data, Novel Technologies, and Modern Systems Engineering. John Wiley & Sons; 2019. p. 273–319.

[3] Singh A, Kapil S, Das M. A comprehensive review of the methods and mechanisms for powder feedstock handling in directed energy deposition. Additive Manufacturing 2020; 35.

[4] Thompson SM, Bian L, Shamsaei N, Yadollahi A. An overview of Direct Laser Deposition for additive manufacturing; Part I: Transport phenomena, modeling and diagnostics. Additive Manufacturing 2015; 8, p. 36–62.

[5] Knüttel D, Baraldo S, Valente A, Bleicher F, Wegener K, Carpanzano E. Machine learning based track height prediction for complex tool paths in Direct Metal Deposition – key opportunities in the tooling industry. To appear on CIRP Annals 2022.

[6] FLOW-3D, https://www.flow3d.com/.

[7] Katopodes ND. Free-Surface Flow – Computational methods. Elsevier; 2019. p. 766–802.

[8] Theofanous T, Biasi L, Isbin HS, Fauske H. A theoretical study on bubble growth in constant and time-dependent pressure fields. Chemical Engineering Science 1969; 24(5), p. 885–897.

[9] ISO 4287:1997, https://www.iso.org/standard/10132.html.

[10] ISO 4288:1996, https://www.iso.org/standard/2096.html.